Thermal analysis of nanofluids in microfluidics using an infrared camera

Pyshar Yi*[a], Aminuddin A. Kayani[a], Adam F. Chrimes[a], Kamran Ghorbani[a], Saeid Nahavandi[b], Kourosh Kalantar-zadeh*[a], and Khashayar Khoshmanesh*[a]

Received (in XXX, XXX) Xth XXXXXXXXX 20XX, Accepted Xth XXXXXXXXX 20XX
DOI: 10.1039/b000000x

We present the thermal analysis of liquid containing Al_2O_3 nanoparticles in a microfluidic platform using an infrared camera. The small dimensions of the microchannel along with the low flow rates (less than 120 µl/min) provide very low Reynolds numbers of less than 17.5, reflecting practical parameters for a microfluidic cooling platform. The heat analysis of nanofluids has never been investigated in such a regime, due to the deficiencies of conventional thermal measurement systems. The infrared camera allows non-contact, three dimensional and high resolution capability for temperature profiling. The system was studied at different *w/w* concentrations of thermally conductive Al_2O_3 nanoparticles and the experiments were in excellent agreement with the computational fluid dynamics (CFD) simulations.

Introduction

In the early 1980s, Tuckerman and Pease carried out experiments to demonstrate the thermal performance of liquid microchannel heat sinks (MCHSs)[1]. This seminal work shaped a new field of research for cooling of microscale electronic devices; especially in large integrated circuits. The idea of implementing MCHSs was revolutionary for its time. In comparison to the fluid cooling systems of that time, the MCHSs allowed for more efficient heat transfer between the cooling liquid and hot-spots, they required much smaller amount of liquid coolant, liquid could be brought to its cool state much easier, and more surface area was available for an efficient heat transfer [2,3].

Even though, liquid cooling is fairly prevalent today, it still requires further development due to the intrinsic poor thermal conductivity of conventional fluids. Thus, the attention is now drawing towards the dispersion of solid particles in liquids to enhance the thermal conductivity and consequently the convection coefficient of the flow[4-11].

The term nanofluids, which introduced by Choi[12], was used for describing stable suspensions of nanometer-sized particles with average dimensions of less than 100 nm in conventional fluids such as water, ethylene glycol or oil. Because nanoparticles such as Al_2O_3, CuO, Cu and TiO_2 have higher thermal conductivities than the base fluids, even at low concentrations, it is believed that nanofluids offer key potential benefits to MHCSs[13-16].

The concept of applying nanofluid coolants in MCHSs has been investigated by different groups[13,16-19]. However, most studies have been performed at high Reynolds numbers ranging from 100 to 2000[17,20,21], corresponding to either MCHSs with large dimensions or high flow rates. The main technical challenge hindering the operation of such systems is their incompatibility to emerging miniaturised electronic systems, as they need large reservoirs and powerful pumps, which defy the purpose of miniaturisation and energy efficiency.

Another issue that has been a serious impediment in exploring the thermal properties of microfluidics with nanofluids has been the lack of suitable methods in measuring temperatures. Thermocouples and thermistors are elements that commonly used to measure the temperature of fluids in microfluidics. They have been widely used by patterning metals incorporated into microchannel[22-24]. However, such elements can only be patterned at limited predetermined locations of the microchannel. Their measurement is restricted to two dimensional surfaces, and one cannot measure the temperature of three dimensional structures accommodating the microchannel. Moreover, thermocouples require extensive wiring. To solve such problems, temperature-dependent fluorescent dyes have been used for the detection of fluids' temperatures in microfludics[25-27]. However, this technique might change the thermophysical properties of the fluid, deteriorating the accuracy of measurements.

Nanofluidics investigations have so far been riddled with practical difficulties. Studies on the thermal characteristics of nanofluids has been mostly based on either pure experimental work[11,14,28] or pure theoretical calculations[18,24,29], which have been incapable to comprehensively demonstrate the performance of such systems.

In our work, we overcome major inaccuracies and problems in exploring microfluidics containing nanofluids. We use a microfluidic system, and integrate it with a microheater and a high resolution infrared (IR) camera. Using the microheater, we are able to accurately control the temperature of the system, and with the IR camera, we can measure the temperatures of any desired location of the microfluidics. Combining these two capabilities, we accurately demonstrate the effect of nanofluids in the thermal performance of the system. We use the suspension of Al_2O_3 nanoparticles, which has a high thermal conductivity, at different concentrations to investigate the enhancement of heat exchange in comparison to DI water as the base fluid. The IR camera allows us to observe the thermal characteristics of the system, even at extremely low Reynolds numbers, the values that are associated with true microfluidics and have not been reported before.

The application of high resolution IR camera enables us to monitor the temperature of desired surfaces at any desired moment. This technique enables us to record the temperature profile of different locations of the microfluidic system, including the 3D structure of the microfluidics block. Advantageously, the measurement is contactless and therefore does not influence the thermal performance of the system. Additionally, the measurement is facile, does not need any specialised training, and enables us to even monitor the dynamic performance of the system.

Our study presents both experimental measurements and numerical simulations to fully understand the response of the system and calculate the heat flux or other variables of the system, which could not be assessed previously.

Theory

Three dimensional numerical simulations were conducted to analyze the variations of velocity, pressure, temperature, and heat loss across the microfluidic system. The highest Reynolds number, $Re=\rho \bar{U} D/\mu$ (ρ is fluid density, $\bar{U}$ is the average fluid velocity, D is the hydraulic diameter of the rectangular microchannel, and μ is the fluid viscosity) obtained at the flow rate of 120 µlit/min is ~17.5, indicating the laminar characteristics of the flow. The simulation was conducted using Gambit 2.3 software (Fluent, Lebanon, NH, USA) to create the geometry and mesh generation. Subsequently, the finite-volume based Fluent 6.3 software (Fluent, Lebanon, NH, USA) was used to solve the associated differential equations governing the balance of mass, momentum, and energy within the microfluidic system, as given by Khoshmanesh *et al*[30].

$$\nabla \cdot \vec{U} = 0 \tag{1}$$

$$\rho\,(\vec{U}\cdot\nabla)\,\vec{U} = -\nabla P + \mu\,\nabla^2\vec{U} \tag{2}$$

$$\rho c_p\ \ (\vec{U}\cdot\nabla)\,T = k\,\nabla^2 T + \dot{Q} \tag{3}$$

where, $\vec{U}$, P and T are the velocity, pressure and temperature of the fluid, ρ, μ, c_p and k are the density, dynamic viscosity, heat capacity and thermal conductivity of the fluid, respectively, and $\dot{Q}$ is the heat source term corresponding to the microheater. The thermophysical properties of nanofluid are obtained as below[31]:

$$\rho_{nf} = (1-\phi)\,\rho_f + \phi\,\rho_p \tag{4}$$

$$\mu_{nf} = \frac{1}{(1-\phi)^{2.5}}\,\mu_f \tag{5}$$

$$(\rho c_p)_{nf} = (1-\phi)(\rho c_p)_f + \phi(\rho c_p)_p \tag{6}$$

$$k_{nf} = \frac{k_p + (n-1)k_f - (n-1)\phi(k_f - k_p)}{k_p + (n-1)k_f + \phi(k_f - k_p)}\,k_f \tag{7}$$

$$n = \frac{3}{\psi} \tag{8}$$

where *f*, *p* and *nf* indices refer to fluid, particle and nanofluid, respectively, Ø is the volume fraction of particles in the suspension, n is the shape factor, and ψ is the sphericity of particles, which was taken as 0.5 due to the non-spherical shape of the particles. The thermophysical properties of the base fluid were taken as ρ_f=998 kg/m^3, μ_f=0.001 Pa.s, c_{pf} =4178 J/kg.K and k_f=0.6 W/m.K while those of Al_2O_3 particles were taken as ρ_p=3950 kg/m^3, c_{pp} =930 J/kg.K and k_p=40 W/m.K.

The Knudsen number, $Kn=2\lambda/d$ (λ is the mean free path length or the average distance between the molecules of DI water and equals to 0.31 nm[32], and d is the average diameter of Al_2O_3 particles and equals to 30 nm) is 0.02 and since it is more than 0.001, the slip boundary condition is applied at the surfaces of the system. In doing so, the slip velocity was defined as below[33]:

$$u_{slip} = L_{slip}\,\lambda\,\frac{\partial u}{\partial n} \tag{9}$$

where L_{slip} is the slip length of PDMS surface taken as 57 nm[34] while $\partial u/\partial n$ is the gradient of flow velocity along the axis normal to the surface.

The other boundary conditions consisted of zero pressure at the inlet and flow rates of 10, 40 and 120 µL/min at the outlet (this is because the suspension is sucked out via the outlet). These flow rates associate with the Reynolds numbers in the range of 1.45 to 17.5. The value of $\dot{Q}$ was obtained by dividing the power supplied to the microheater (by reading the voltage and current of the DC power supply) by the volume of the microheater. The voltage was changed to maintain the temperature of the microheater centre at 54°C. The external surfaces of the system exchanged heat with the ambient air *via* the free convection mechanism assuming the convection coefficient as 10 W/m^2.K while the ambient temperature was measured as 25.8˚C. The heat passed through the walls of the glass slide and PDMS *via* the conduction mechanism with k_{glass}=1.05 W/m.K and k_{PDMS}=0.15 W/m.K.

Experimental

Apparatus

The schematic of the experimental setup is shown in Fig. 1(A) (refer to Fig. 1S for the real experimental setup). The system consisted of a polydimethylsiloxane (PDMS) block integrated onto a microscopic glass slide, as shown in Fig. 1(B). The PDMS hosted a microchannel and two reservoirs as the inlet/outlet of the microchannel, as seen in Fig. 1(C). The glass slide accommodated a metallic microheater patterned on its surface as shown in Fig. 1(D). The flow was provided through the microchannel *via* a syringe pump (Harvard, PHD 2000 Infusion). The syringe pump was activated in refill mode to supply suction, avoiding the leakage and generation of bubbles within the microchannel. The microheater was energised *via* a DC power supply (Gw Instek, GPS-X303 series, Taiwan) and was used to heat up the liquid to the desired temperatures before entering the microchannel.

The temperature measurement along the bottom glass surface that covered the microchannel (Fig. 1(C)) was recorded using an IR camera (FLIR Systems, ThermoVision A320, Sweden) interfaced with ThermaCAM Researcher software. The microfluidic device was rotated upside down such that the glass substrate was immediately facing the camera, as shown in Fig. 1(A).

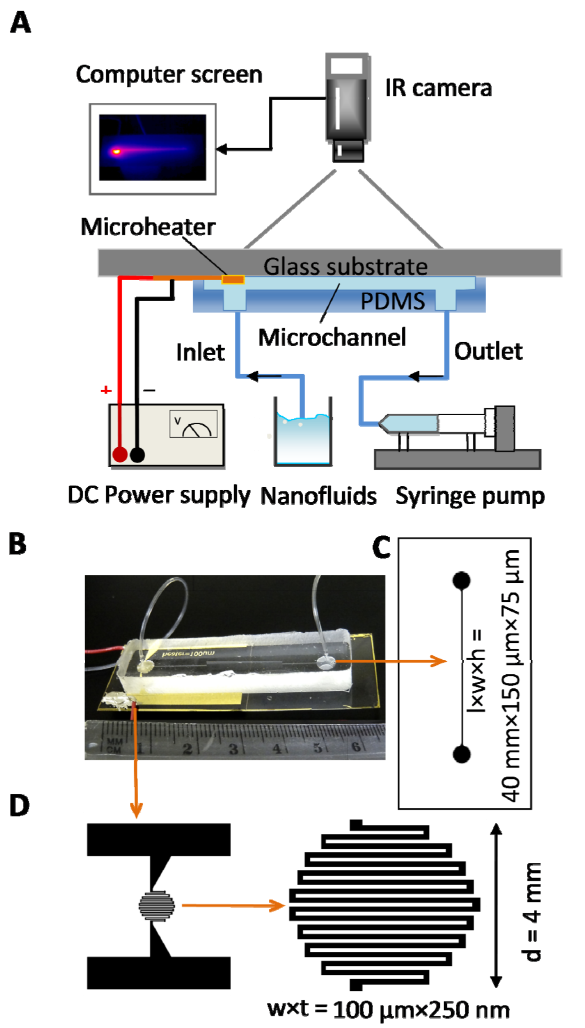

Fig. 1. (A) Schematic of the setup for investigation of nanofluid on heat transfer enhancement consisted of: (B) Microfluidic device, (C) Microchannel design and (D) Microheater pattern.

Nanofluid preparations

Nanosized, Al_2O_3 powders of the diameters of 50 nm or less were purchased from Sigma-Aldrich, Australia. Al_2O_3 was chosen as it has the thermal conductivity of 40 W/mK in comparison to DI water of 0.613 W/mK[35]. Al_2O_3 powder was suspended in DI water at room temperature to create a final solution of 1 and 2.5% *w/w* concentrations. A liquid surfactant (Triton X-305) of 0.2% *w/w* was added to produce a stable suspension; followed by 20 minutes sonication using an ultrasonic bath (Unisonics, Australia). The dimensions of nanoparticles were confirmed by high resolution scanning electron microscopy (FEI Nova NanoSEM, USA) imaging to be mostly smaller than 50 nm (Fig. 2). The dynamic light scattering also confirmed that nanoparticles have an average dimension of ~35 nm.

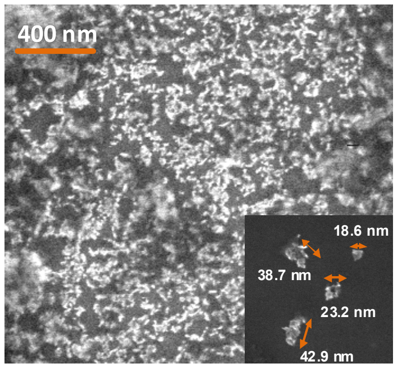

Fig. 2. SEM image of Al_2O_3 nanoparticles

Design Details of Microfluidic Chip

The microchannel was fabricated from PDMS using soft photolithography techniques[36,37]. In doing so, SU8-2050 (Microchem, USA) layer was spin coated on a 3-inch diameter silicon wafer to produce a 75 µm thickness layer. The sample was then exposed to UV light source using an MA6 mask aligner for 28 seconds, and developed in SU-8 developer to recognize the patterns on the master. A 10 g mixture of PDMS (SYLGARD 184, Dow Corning, USA) base and curing agent was mixed in 10:1 weight ratio, and degassed to remove the trapped air bubbles using a vacuum oven. The PDMS mixture was transferred onto the master and cured in an oven with a temperature of 70°C for 20 minutes. The substrate was allowed to cool down for 5 minutes. The PDMS block of 50 mm × 10 mm × 5 mm (length×width×height) was carefully peeled from the master. The microchannel dimensions were set to 150 µm × 75 µm × 40 mm (width × height × length). The channel's height of 75 µm was chosen to allow a free flow of naonoparticles with sizes less than 50 nm and prevent clogging.

The PDMS block was integrated onto a glass slide (Menzel-Glaser, USA) of 60 mm × 20 mm × 100 µm (length × width × height). The glass thickness of 100 µm was chosen to facilitate the exchange of heat between the liquid and the environment, as well as allowing the most efficient observation using the IR camera. The microheater was patterned onto the glass substrate using photolithography. In doing so, thin layers of Au/Cr (150/100 nm) were deposited on the glass surface using electron beam evaporation process. Next, the substrate was spun coated with AZ1512 photo-resist using a spinner (Karl Suss RC8). This substrate was baked in an oven at 90 ºC for 20 minutes, before exposure to UV light through a PDF mask. Subsequently, the exposed substrate was developed in AZ400K developer and a gold etchant (niro-hydrochloric acid, 1:4 *v/v* ratios) was applied to etch the unwanted gold. The substrate was rinsed and cleaned using acetone, methanol and DI water. A chromium etchant was then used to remove the excess chromium.

The substrate was again cleaned with acetone, methanol, DI water and air dry. The fabrication process was conducted in a class 1000 cleanroom. Microtubes with an internal diameter of ~400 µm were placed into the holes punched of the PDMS. These tubes allowed the interfacing of syringe pumps and samples with the microchannel.

Measurements

First, we investigated the thermal performance of our microfluidic system using DI water as the working fluid at a flow rate of 40 µlit/min. We placed the IR camera at a distance of 0.3 m from any surface of the microfluidic system which we were interested to measure its temperature. The voltage of DC power supply was varied to provide a constant temperature of 54 °C at the middle of the inlet reservoir when seen from the glass side. The temperatures were recorded in 90 second frames using the IR camera and the images were extracted from the last frame. Examples of these measurements are shown in Fig. 3(A-C). As clearly seen in the images, the IR camera enables us to observe how the heat is dissipated within the PDMS block, the glass slide, and more importantly throughout the microchannel. We also compared the measured temperature with results of CFD simulations, as shown in Fig. 3(D-F). The colours of the temperature bar are selected to match with the IR camera settings. However, the exact comparison between the experimental and numerical results is given later.

Next, we moved on to characterise the thermal performance of our microfluidic system at different flow rates and concentrations of Al_2O_3 nanoparticles.

Figs. 4(A-C) show the temperature profiles across the glass slide (the bottom view) after applying only DI water through the system at different flow rates of 10, 40 and 120 µlit/min. These figures clearly show the extension of golden (50-40°C) and pink (40-30°C) regions throughout the glass surface by increasing the flow rate. Obviously at higher flow rates convection becomes the dominant mode of heat transfer along the microchannel, as the liquid does not have enough time to lose its internal heat to the environment *via* the channel surfaces.

Figs. 4(D-F) show the temperature profiles across the glass slide (the bottom view) after applying DI water and water mixed with Al_2O_3 concentrations of 1% and 2.5% *w/w* at a constant rate of 40 µlit/min. By careful examination of the temperature contours one can see their changes due to incorporation of nanoparticles. As can be seen, the increased thermal conductivity of liquid with 2.5% *w/w* Al_2O_3 increases the heat conduction along the microchannel, reducing the temperature gradient along the length.

To quantify the thermal impact of the nanoparticles, we investigated the variations of temperature along the microchannel centreline. In doing so, we defined 38 points along this line and read their temperatures using the images obtained from the IR camera. Fig. 5(A) shows the variations of temperature along this centreline of the microchannel at different flow rates of 10, 40 and 120 µlit/min and different Al_2O_3 concentrations of 0%, 1% and 2.5% suspended in DI water.

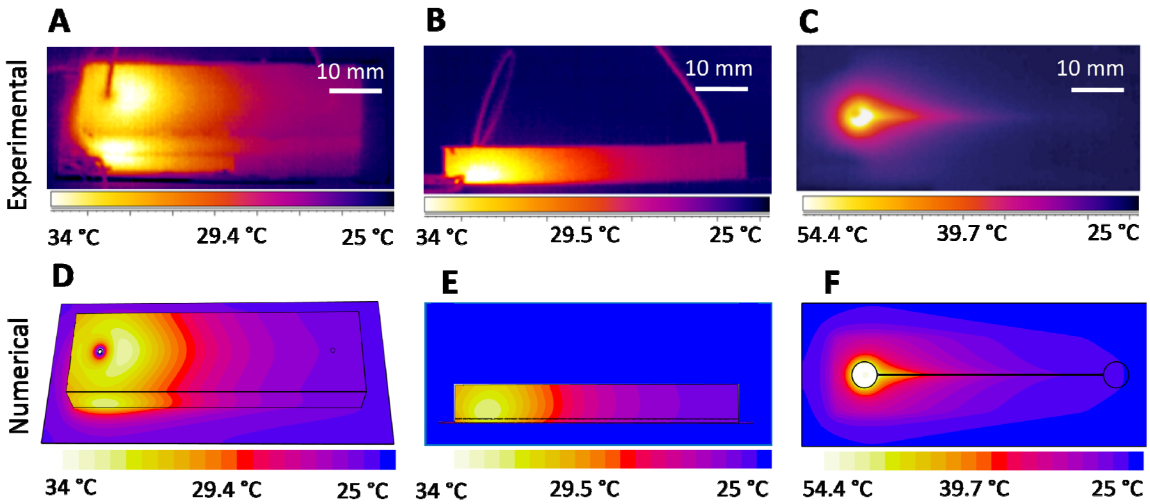

Fig. 3. Temperature distribution across the external surfaces of the microfluidic system with DI water at a flow rate of 40 µlit/min. Measured temperatures using infrared camera: (A) 3D view, (B) side view and (C) bottom view, Calculated temperatures using CFD simulations: (D) 3D view, (E) side view and (F) bottom view.

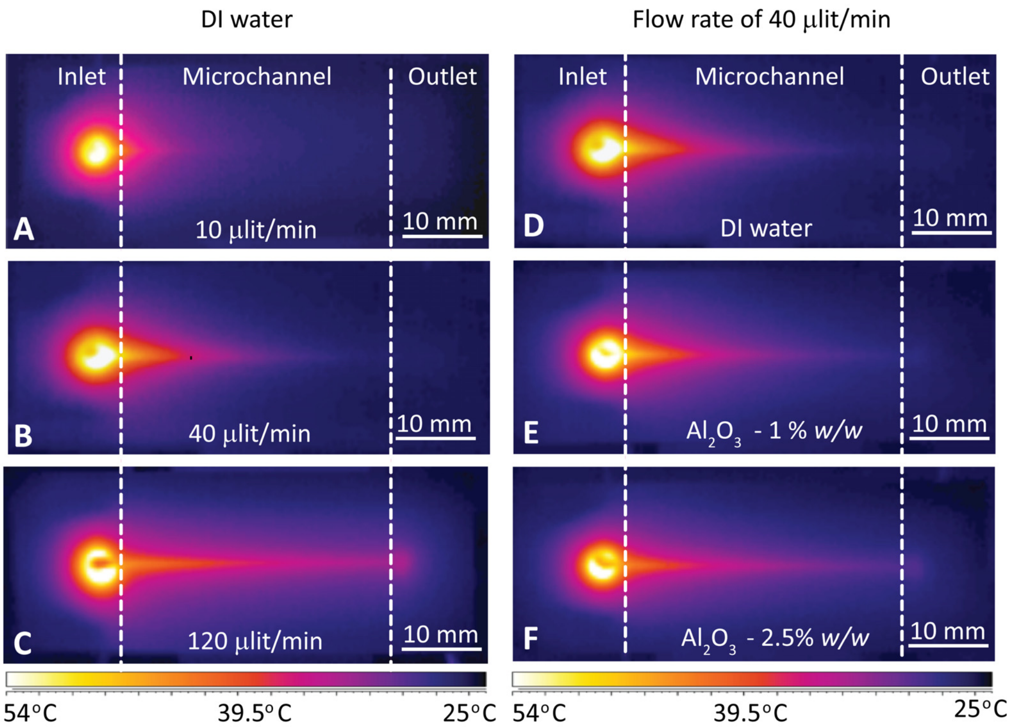

Fig. 4. Temperature distribution across the bottom surface of glass slide: (A-C) DI water as the working fluid at different flow rates of 10, 40 and 120 µlit/min, (D-F) DI water with different Al_2O_3 concentrations of 0%, 1% and 2.5% *w/w* at a constant flow rate of 40 µlit/min

Results and Discussions

Fig. 5(A) shows the outcomes of measurements only. This figure demonstrates that the temperature drop, along the microchannel centreline, decreases significantly by increasing the flow rate of DI water and liquid suspensions incorporating Al_2O_3 nanoparticles, indicating the enhancement of convection within the microchannel at higher flow rates. For example, for the case of DI water, while a temperature drop of 28°C was observed along the centreline at 10 µlit/min, it reduced to 25°C at 40 µlit/min and further reduced to 21°C at 120 µlit/min. Similar trends can be seen for other concentrations of Al_2O_3. Fig. 5(A) also shows that the temperature drop along the microchannel decreases by increasing the concentration of Al_2O_3, indicating the superior thermal conductivities of nanofluids. For example at 10 µlit/min, while a temperature drop of 28.2°C was observed along the centreline for DI water, it reduced to 27.6°C for the 1% Al_2O_3 suspension and further reduced to 27.4°C for the 2.5% Al_2O_3 suspension. Interestingly, the effectiveness of nanofluids was more tangible at higher flow rates. For example at 120 µlit/min, while a temperature drop of 22.7°C was observed along the centreline for DI water, it reduced to 21.6°C for the 1% Al_2O_3 suspension and further reduced to 19.5°C for the 2.5% Al_2O_3 suspension.

Figs. 5(B-C) compare the variations of experimental and simulated temperatures along the centreline. Results show an excellent agreement between the experimental and numerical results. In general, the calculated temperatures were slightly lower at the inlet of the microchannel, while rather smaller at the outlet of the microchannel.

Next, we investigated the variations of heat flux along the centreline using our CFD model, as shown in Fig. 6. As before, we examined different flow rates of 10, 40 and 120 µlit/min and different Al_2O_3 concentrations of 0%, 1% and 2.5% suspended in DI water. According to the simulations, at a low flow rate of 10 µlit/min, the addition of nanoparticles did not have a considerable effect on the heat flux curves and only slightly improved the heat flux at the inlet of the microchannel.

Increasing the flow rate to 40 µlit/min, the average heat flux increased by 6.5% for the 1% Al_2O_3 suspension and by 13.5% for the 2.5% Al_2O_3 suspension. Similarly, increasing the flow rate to 120 µlit/min, the average heat flux increased by 10.8% for the 1% Al_2O_3 suspension and by 23.5% for the 2.5% Al_2O_3 suspension.

Obviously, the outcomes show that the incorporation of the thermally conductive nanoparticles enhances the heat exchange between the working fluid and its environment, resulting in the efficient cooling of the system when it is required.

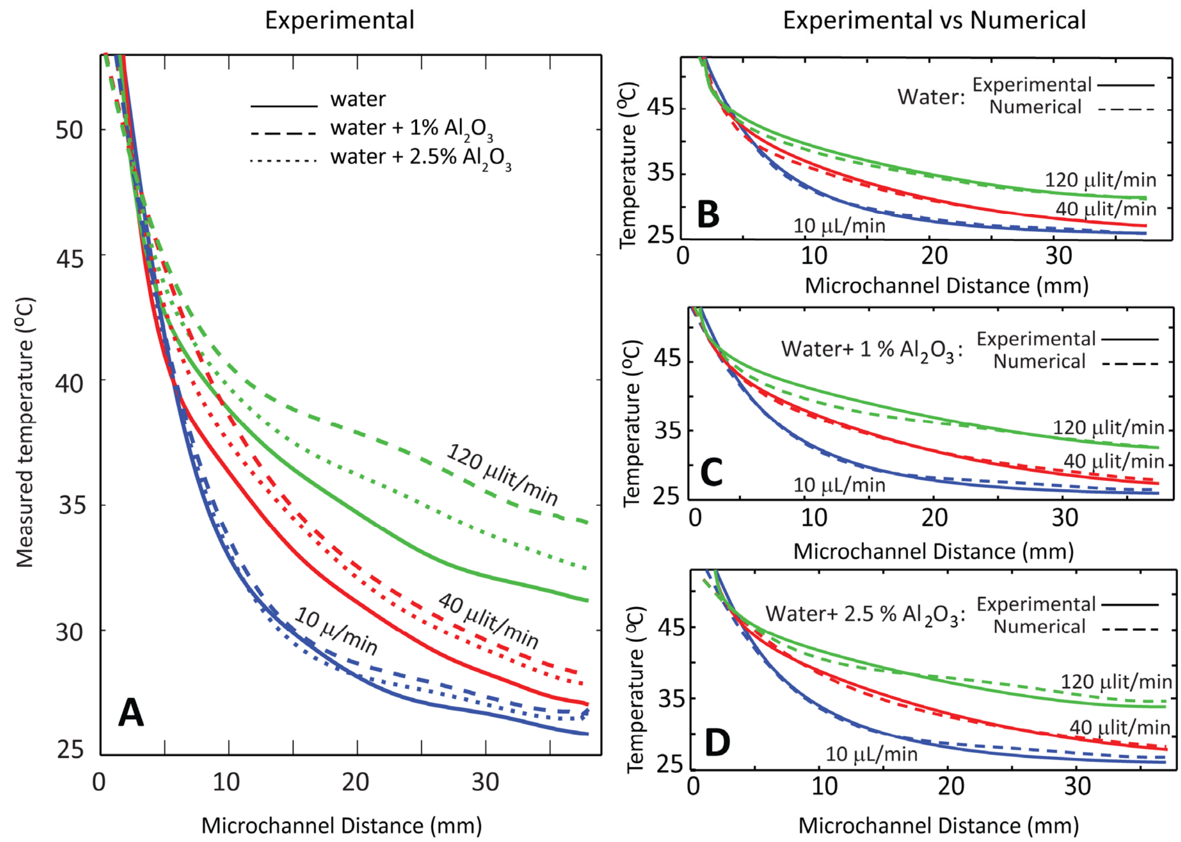

Fig. 5. Variation of temperature at the bottom surface of the microfluidic system along the centreline: (A) Experimental temperatures at the flow rates of 10, 40 and 120 µlit/min, and different *w/w* Al_2O_3 concentrations of 0%, 1% and 2.5%. (B-D) Experimental versus numerical temperatures at 10, 40 and 120 µlit/min for (B) DI water, (C) water plus 1% *w/w* Al_2O_3 and (D) water plus 2.5% *w/w* Al_2O_3.

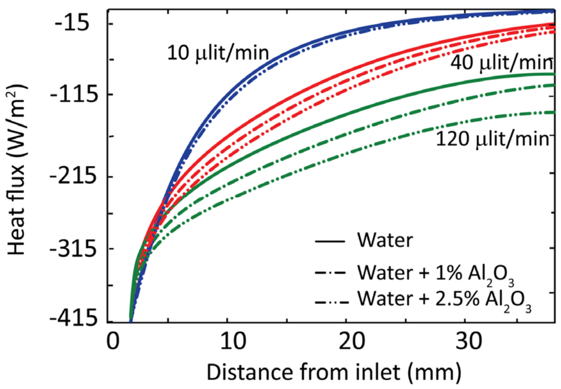

Fig. 6. Heat flux profile along the centreline at different flow rates and various concentrations of Al_2O_3 nanoparticles.

Conclusion

The work is a comprehensive analysis of heat transfer in a true micofluidic system with and without suspended Al_2O_3 nanoparticles. According to our observations, at low flow rate of 10 µlit/min, associated with the Reynolds number of 1.45, no significant difference was observed between the conventional fluid and nanofluids, as also confirmed by the numerical simulations. In contrast, at higher flow rates of 120 µlit/min, associated with the Reynolds number of 17.5, the exchange of heat for the liquid with nanoparticles was much enhanced. All the observations were based on the incorporation of an IR camera for measuring the temperature profiles, which was non-contact without affecting the thermal properties of the platform. Further improvement of the system is needed to account for a number of factors such as the investigation of different sizes and types of nanoparticles as well as the modification of the microchannel design in order to obtain higher heat transfer efficiencies.

As nanoparticles are becoming more readily accessible, their application in microfluidics is becoming increasingly attractive. Future Very Large Scale Integration (VLSI) of electronic elements requires exceedingly more components, and consequently more efficient cooling systems. Nanofluids will certainly play an important role in providing solutions for the cooling issues of such complex systems.

Notes and references

[a] *RMIT University, School of Electrical and Computer Engineering, Melbourne, Victoria, Australia. Tel: (03) 992 53254. E-mail: pyshar.yi@gmail.com, kourosh.kalantar@rmit.edu.au and khashayar.khoshmanesh@rmit.edu.au*
[b] *Centre for Intelligent Systems Research, Deakin University, Victoria, Australia.*

† Electronic Supplementary Information (ESI) available: [Experimental setup] see DOI: 10.1039/b000000x/

.1. D. B. Tuckerman and R. F. W. Pease, *Electron Device Letters*, 1981, **2**, 126-129.
2. D. Erickson, D. Sinton and D. Q. Li, *Lab on a Chip*, 2003, **3**, 141-149.
3. J. Atencia and D. J. Beebe, *Nature*, 2005, **437**, 648-655.
4. M. P. Beck, T. F. Sun and A. S. Teja, *Fluid Phase Equilibria*, 2007, **260**, 275-278.
5. H. Q. Xie, J. C. Wang, T. G. Xi, Y. Liu, F. Ai and Q. R. Wu, *Journal of Applied Physics*, 2002, **91**, 4568-4572.
6. W. Yu and S. U. S. Choi, *Journal of Nanoparticle Research*, 2003, **5**, 167-171.
7. S. M. S. Murshed, K. C. Leong and C. Yang, *International Journal of Thermal Sciences*, 2005, **44**, 367-373.
8. S. Movahed and D. Li, *Electrophoresis*, 2011, **32**, 1259-1267.
9. S. Ozerinc, S. Kakac and A. G. Yazicioglu, *Microfluidics and Nanofluidics*, 2009, **8**, 145-170.
10. C. L. Altan and S. Bucak, *Nanotechnology*, 2011, **22**, 285713
11. C. H. Li and G. P. Peterson, *Journal of Applied Physics*, 2006, **99**.
12. S. U. S. Choi, *Developments and Applications of Non-Newtonian Flows*, 1995, **231, ASME**, 99-105.
13. H. A. Mohammed, P. Gunnasegaran and N. H. Shuaib, *International Communications in Heat and Mass Transfer*, 2011, **38**, 194-201.
14. R. Chein and J. Chuang, *International Journal of Thermal Sciences*, 2007, **46**, 57-66.
15. R. Y. Chein and G. M. Huang, *Applied Thermal Engineering*, 2005, **25**, 3104-3114.
16. T. H. Tsai and R. Chein, *International Journal of Heat and Fluid Flow*, 2007, **28**, 1013-1026.
17. H. A. Mohammed, P. Gunnasegaran and N. H. Shuaib, *International Communications in Heat and Mass Transfer*, 2011, **38**, 767-773.
18. E. Farsad, S. P. Abbasi, M. S. Zabihi and J. Sabbaghzadeh, *Heat and Mass Transfer*, 2011, **47**, 479-490.
19. H. A. Mohammed, P. Gunnasegaran and N. H. Shuaib, *International Communications in Heat and Mass Transfer*, 2010, **37**, 1496-1503.
20. X. Wu, H. Wu and a. P. Cheng, *Journal of Micromechanics Micorengineering*, 2009, **19**.
21. D. S. Wen and Y. L. Ding, *Microfluidics and Nanofluidics*, 2005, **1**, 183-189.
22. U. Seger-Sauli, M. Panayiotou, S. Schnydrig, M. Jordan and P. Renaud, *Electrophoresis*, 2005, **26**, 2239-2246.
23. P. B. Allen, I. Rodriguez, C. L. Kuyper, R. M. Lorenz, P. Spicar-Mihalic, J. S. Kuo and D. T. Chiu, *Analytical Chemistry*, 2003, **75**, 1578-1583.
24. Q. Z. Xue, *Physics Letters A*, 2003, **307**, 313-317.
25. D. Ross, M. Gaitan and a. L. E. Locascio, *Analytical Chemistry*, 2001, **73**, 4117-4123.
26. R. Fu, B. Xu and D. Li, *International Journal of Thermal Sciences*, 2006, **45**, 841-847.
27. A. Gunther, S. A. Khan, M. Thalmann, F. Trachsel and a. K. F. Jensen, *Lab on a Chip*, 2004.
28. S. Shaikh, K. Lafdi and R. Ponnappan, *Journal of Applied Physics*, 2007.
29. P. Bhattacharya, A. Samanta and S. Chakraborty, *Heat and Mass Transfer*, 2009, **45**, 1323-1333.
30. K. Khoshmanesh, J. Akagi, S. Nahavandi, J. Skommer, S. Baratchi, J. M. Cooper, K. Kalantar-zadeh, D. E. Williams and D. Wlodkowic, *Analytical Chemistry*, 2011, **83**, 2133-2144.
31. A. Ijam and R. Saidur, *Applied Thermal Engineering*, 2012, **32**, 76-82.
32. S. J. Perkins, *European Journal of Biochemistry*, 1986, **157**, 169-180.
33. A. Moshfegh, M. Shams, G. Ahmadi and R. Ebrahimi, *Colloids and Surfaces A: Physicochemical and Engineering Aspects*, 2009, **345**, 112-120.
34. P. Huang, J. S. Guasto and K. S. Breuer, *Journal of Fluid Mechanics*, 2006, **566**, 447-464.
35. S. Kakaç and A. Pramuanjaroenkij, *International Journal of Heat and Mass Transfer*, 2009, **52**, 3187-3196.
36. K. Kalantar-zadeh, K. Khoshmanesh, A. A. Kayani, S. Nahavandi and A. Mitchell, *Applied Physics Letters*, 2010, **96**.
37. A. F. Chrimes, A. A. Kayani, K. Khoshmanesh, P. R. Stoddart, P. Mulvaney, A. Mitchell and K. Kalantar-zadeh, *Lab on a Chip*, 2011, **11**, 921-928.